Broadband THz Pulse Transmission Through the Atmosphere

Yihong Yang, *Student Member, IEEE*, Mahboubeh Mandehgar, and Daniel R. Grischkowsky, *Fellow, IEEE*

(Invited Paper)

***Abstract*—We have transmitted a low-power beam of repetitive broadband THz pulses the record distance of 167 m through the atmosphere with 51% relative humidity at 21 °C and have observed the broadened transmitted pulses with a signal to noise ratio greater than 200. The measured transmitted pulses reshaped from a 0.5-ps input pulse into an output pulse structure with a 5-ps symmetric pulse at the leading edge followed by a frequency-swept, rapidly oscillating trailing edge extending with increasing frequency to beyond 150 ps. The leading pulse appearing in the output pulse structure is composed of phase-locked frequency components extending from 0.07 to 0.37 THz that experienced negligible attenuation and group velocity dispersion due to transmission through water vapor. Such a stable pulse shape is suitable for the THz bit in a digital THz communications channel. Our results demonstrate a bit rate-distance product of greater than 8 (Gb/s)-km, which is comparable to an optical fiber digital communications channel.**

***Index Terms*—Absorption, atmospheric transmission, spectroscopy, Terahertz communication, Terahertz.**

I. Introduction

EVER since the initially unexplainable demonstration of the transmission of electromagnetic waves across the Atlantic Ocean by Marconi in 1901, understanding the propagation of freely propagating electromagnetic waves within the atmosphere has been key to major advances in communications. In Marconi's case, the accidental discovery of the ionosphere provided the explanation for his remarkable achievement. However, in contrast to the enabling influence of the ionosphere, the effects of water vapor in the atmosphere have created many impossibilities for electromagnetic communications. In the frequency range from 0.1 to 10 THz, the absorption and group velocity dispersion (GVD) of water vapor controls the propagation of THz waves in the atmosphere. The variable amount of water vapor in the atmosphere determines the feasibility of proposed research, technical and commercial applications of THz electromagnetic wave transmission. The absolute humidity changes strongly with the daily weather, changing seasons, altitude, and geographical location.

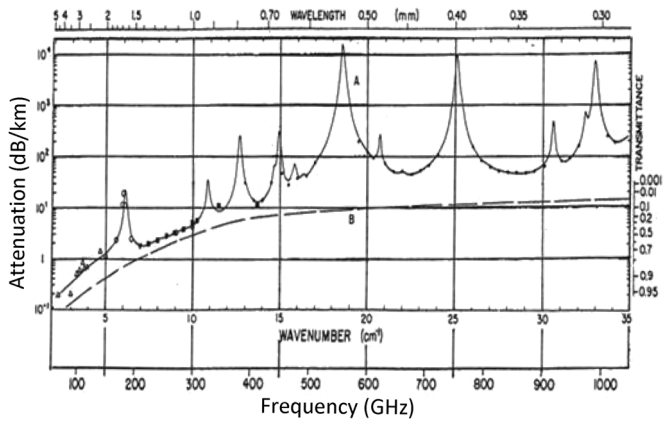

Fig. 1. This figure is a revised version of Fig. 10 of [5] with the caption, "Spectral plots of the near-millimeter attenuation by the atmospheric H_2O at sea level. H_2O density $= 5.9\ g/m^3$. Curve A represents attenuation calculated by summing the theoretical contributions by all the lines and adding the continuum represented by curve B" [5]. The H_2O density corresponds to a relative humidity of 34% at 20° C. The indicated measurements have been done by several groups; the open triangles below 150 GHz are from Dryagin *et al.* [6]; the open circles below 200 GHz are from Frenkel and Woods [7]; the filled triangle at 200 GHz is from Straiton and Tolbert [8]; the filled squares from 200 to 400 GHz are from Ryadov and Furashov [9], and the solid circles from below 400 GHz to 1000 GHz are from Burch [10], [11].

The historic Fig. 1 shows the enormous variation of THz power attenuation (dB/km) over the frequency range from 100 GHz (0.1 THz) to 1000 GHz (1 THz) [1]. The attenuation changes by five orders of magnitude from maximum to minimum over this frequency range. Curve A in Fig. 1. is the sum of the calculated attenuation of all the water rotational lines, plus the much weaker continuum attenuation shown as curve B, which is considered to be due to water dimers, higher order clusters, and self-broadening of the strong water lines [1]–[5].

Many simulation codes have been developed to model the absorption of THz radiation by water vapor in the atmosphere [1]–[4]. The early high quality work to understand the propagation of near-millimeter (100 GHz to 1000 GHz, 0.1 THz to 1 THz, 3 to 0.3 mm) is well detailed in the 1979 *Proceedings of the International Workshop on Atmospheric Water Vapor* [1], which includes both theoretical and experimental investigations of water vapor in the atmosphere. This workshop was stimulated by "The DARCOM/DARPA

Manuscript received March 21, 2011; accepted May 26, 2011. Date of current version August 31, 2011. This work was partially supported by the DTRA (10-2960M), the Air Force Research Laboratory (AFRL), and the National Science Foundation.

The authors are with the School of Electrical and Computer Engineering, Oklahoma State University, Stillwater, OK 74078 USA (e-mail: daniel.grischkowsky@okstate.edu).

Color versions of one or more of the figures in this paper are available online at http://ieeexplore.ieee.org.

Digital Object Identifier 10.1109/TTHZ.2011.2159554

Near-Millimeter Wave Technology Base Study"[1] [2]. Fig. 1 is a revised version of a similar figure that appeared in both [1] and [2]. In particular, our Fig. 1 is a revised version of Fig. 10 of [5] showing the measured and calculated attenuation from 100 to 1000 GHz of atmospheric water vapor with a density of 5.9 g/m^3, corresponding to a relative humidity of 34% at 20 °C. The indicated measurements on Fig. 1 have been done by many different groups [6]–[11], and their impressive accuracy presents a challenge to the recently developed optoelectronic, coherent, high-signal-to-noise technique of terahertz time-domain spectroscopy (THz-TDS) [12]–[14].

Previous short-path THz-TDS measurements have characterized the strong rotational lines of the water vapor spectrum [12], [15], and thereby again presented the transparent window regions [11], [15]. A recent THz-TDS measurement of the amplitude transmission of a 1-m-long atmospheric path provides meaningful results from 1 to 3 THz [16]. There has been a significant demonstration of broadband THz pulse transmission through the ground level atmosphere for the record long path of 108 m [17], although most of the observed low-frequency attenuation was due to the frequency-dependent power transfer losses in the optical train involving more than 30 mirrors. A most recent THz-TDS measurement has characterized atmospheric water vapor from 0.2 to 2 THz with a 6.2-m path length at RH 51% [18].

In this paper, we describe an investigation of the limits of short broadband THz pulse propagation in the atmosphere using a low-power, high signal-to-noise ratio (S/N) coherent optoelectronic system. Our goals were to assess the practical bandwidth and distance for atmospheric sensing, ranging, and communications with a well-coupled and -understood THz optical system. Given sufficient stability, we also planned to make highly accurate measurements of the attenuation of the atmosphere due to water vapor. For our experimental investigation, we transmitted a 30-nW beam of 0.5-ps THz pulses with a repetition rate of 89.82 MHz through the record setting round-trip path of 167 m. The output pulses with unprecedented S/N were measured and compared to the input pulse. We used the THz-TDS coherent, optoelectronic technique [13], [14] that measures the electric field of the THz pulses. Consequently, a numerical complex Fourier transform of the measured THz pulse gives the corresponding amplitude and phase of all the frequency components.

We will initially describe the measurements of the high S/N THz pulses that have been transmitted through 167 m of the atmosphere. We will then describe the unique THz long-path system in much detail and analyze its performance. Finally, we will describe the THz applications that are shown to be possible by our results. In particular, we describe our characterization of the THz communications channel of the atmosphere.

[1]The study consists of three volumes—Vol. I. "Propagation and Target/Background Characteristics," Vol. II, "Components," and Vol. III, "Applications" (1978). In early 1977, interest in the properties of the atmosphere for propagation of electromagnetic waves with wavelengths near 1 mm initiated a comprehensive study of the status and projected future of millimeter/submillimeter technology. With DARCOM (U.S. Army Materiel Development and Readiness Command) and DARPA (Defense Advanced Research Projects Agency) support, a distinguished group of 50 knowledgeable scientists and engineers met many times over a nine-month period to complete this study. The panel's efforts were focused on the properties of the atmosphere for frequencies between 100 to 1000 GHz (0.1 to 1 THz, 3 to 0.3 mm). At that early time, this frequency region brought together the fields of microwaves and optics.

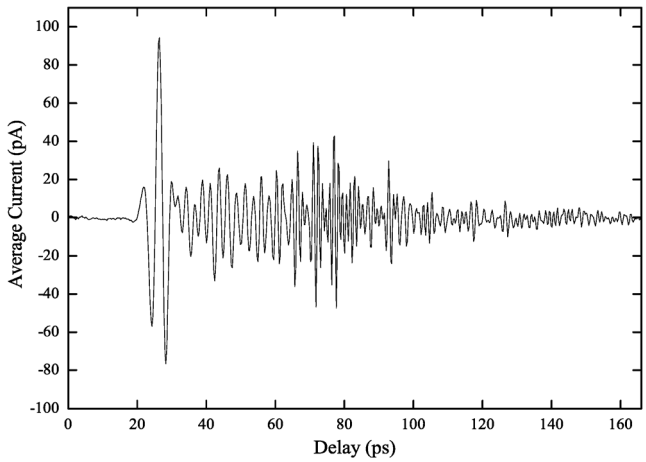

Fig. 2. Measured THz pulse transmitted through the 167-m path with relative humidity of 51% at 21 °C.

II. Experimental Setup and Measurements

The repetitive, broadband, THz pulse of the low-power THz beam transmitted through 167 m of the atmosphere at 51% relative humidity (RH) is shown with an S/N greater than 200 in Fig. 2. The output pulse appears as an initial pulse followed by an extensively broadened and frequency swept trailing edge due to the GVD of water vapor. These pulses have a transmitted bandwidth from 0.1 to 1 THz and were measured using the relatively well-coupled system shown in Fig. 3. These observations show the practicality of THz transmission through the windows of transparency between the water lines within this bandwidth [1]–[4], [18].

The input pulse (to mirror M1 in Fig. 3) had a 0.5-ps pulsewidth with a peak-to-peak amplitude of 6000 pA compared to 200 pA in Fig. 2. The input THz pulse train had an average power of approximately 30 nW [13], [19], compared to the average power of 130 pW for the transmitted pulses shown in Fig. 2. The transmitted power was obtained by comparing the integrals of the power spectrum of the input pulse to that of the pulse shown in Fig. 2. The long-path pulse power has been reduced by the output and input coupling, diffraction loss, and water vapor absorption.

The combination of THz optics with synchronously gated, optoelectronic detection has exceptional sensitivity for repetitively pulsed beams of THz radiation. Using collimating, focusing, and flat mirrors, it is possible to direct a relatively large fraction of the THz radiation, emitted by the ultrafast laser excitation of the optoelectronic transmitter, onto a distant target. The burst of THz radiation emitted by the Hertzian dipole antenna is collimated by the THz optical system into a diffraction-limited beam, which is coupled into the long-path system and returned with good coupling efficiency into the THz receiver. The resulting tightly coupled system of the THz transmitter and receiver (transceiver) gives strong reception of the transmitted pulses of THz radiation after 167 m of propagation through the atmosphere.

A major reason for the exceptional sensitivity is the synchronous optoelectronic gating of the receiver with the short gating window of 0.6 ps, determined by the 80-fs laser pulses and the photocarrier lifetimes of 600 fs [20]. Consequently, noise is not measured during the 11.1 ns between the repetitive THz pulses, but only during the 0.6-ps gating window driven by the ultrafast laser gating pulses. Another important feature is that the detection method is a coherent process; the electric field of the repetitive pulses of THz radiation is directly measured. Because the repetitive signal is synchronously measured, the total charge (current) from the signal current amplifier increases linearly with the number of sampling pulses, while the charge (current) from noise increases only as the square root of the number of pulses.

To operate the THz-TDS system as a THz transceiver, only modest ultrafast pumping power was needed for our measurement; a 10-mW laser beam pumped the THz transmitter and another 10-mW laser beam pumped the THz receiver. The optoelectronic system is described in [13] and [14]. In summary, the THz pulses are generated by the 10-mW optical pulse train from an 850-nm, 80-fs, 89.82-MHz mode-locked Ti–Sapphire laser driving the optoelectronic source chip. The generated THz beam is collimated by a high-resistivity silicon truncated spherical lens with a 5-mm radius of curvature and thickness of 6.56 mm. The flat surface of this lens is attached to the back side of the source chip. The front spherical surface of the lens is located at the 119-mm focus of a 75-mm-diameter paraboloidal mirror. This paraboloidal mirror gently focuses the generated THz beam to the beam waist at the focal plane midway between the two identical paraboloidal mirrors shown in the insert in Fig. 3. The Gaussian beam waist diameter is proportional to wavelength and is 10 mm at 1 THz. The receiver optics are the same with a matching paraboloidal mirror, silicon lens, and optoelectronic receiver chip.

In order to have the high S/N of coherent sampling, the propagation distance of 166.84 m was chosen to be precisely equal to an integer number of round-trips (50 for this case) of the ultrafast optical pulses in the mode-locked Ti–Sapphire pumping laser. This laser has a repetition rate of 89.82 MHz determined by the measured round-trip distance of 333.7 cm. Consequently, the laser sampling pulses, used to measure the THz pulses that have propagated 166.84 m, are delayed by 50 pulses down the pulse train from the excitation pulses. The fact that we can measure to ps precision, shows that the THz optical train is surprising stable, even though the mirror mount supports for M5–M9 (shown in Fig. 3) are placed on the stable floor of our basement laboratory. Mirrors M1–M4 and M10 are on the optical table.

However, there was a slow thermal drift of the measured pulse of approximately 0.6 ps/hour, which corresponds to only a 180-μm/h change in the THz long-path length compared to the corresponding length of 50 laser round-trips. Because the thermal drift is quite slow compared to a THz pulse measurement that requires only three minutes, it is possible to numerically align a series of pulse measurements for time-domain averaging. The alignment to adjust the peaks of the pulses to be coincident is done by adding or dropping zeros at the start or at the end of the individual scan's time domain data array. The number of elements in the data array is kept constant. The corresponding amplitude Fourier transforms do not change with pulse drift, and simple averaging is effective.

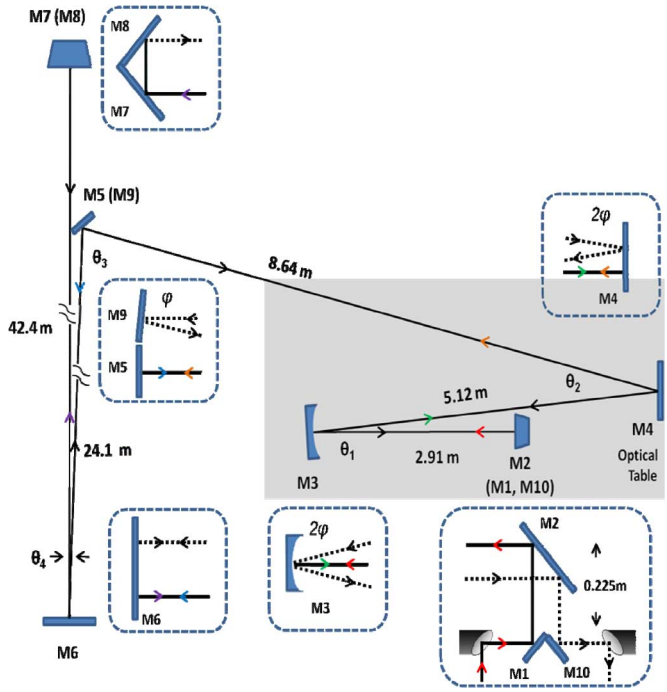

Fig. 3. Top (x–z plane) view of the long-path THz transmission setup. Insets: Side (y–z plane) views of all mirrors. Solid lines show the optical path and the outgoing THz beam (in insets); dashed lines show the incoming THz beam. Arrows indicate THz beam directions, colors distinguish overlapping beams in side view. The indicated angles are $\theta_1 = 5.4°$; $\theta_2 = 19°$; $\theta_3 = 80°$; $\theta_4 = 2.4°$; and $\varphi = -1.25°$, vertical tilt for receiver coupling.

The THz pulses are outcoupled vertically from the THz-TDS system by mirror M1, as shown in the Fig. 3 inset. The reflection from Mirror M2 initiates the elevated horizontal beam line (in the x–z plane) to the 32-cm (12.5 in) diameter, collimating mirror M3 with a focal length of 318 cm (125 in) and the corresponding radius of curvature of 635 cm (250 in). The focus of M3 is located at the confocal THz beam-waist of the THz-TDS system, for which the Gaussian beam-waist diameter is proportional to wavelength and is 10 mm at 1 THz. The reflected and collimated beam from M3 is directed to M4. The reflected THz beam from M4 is directed within the x–z plane to mirror M5, which, in turn, reflects the beam horizontally in the x–z plane to tall mirror M6. From M6, the beam is directed horizontally to M7. As shown in the inset, in order to spatially separate the returning and outgoing beam, mirror M7 reflects the beam vertically up 30.5 cm (12 in) to the upper mirror M8, which reflects the beam horizontally to tall mirror M6. Mirrors M7 and M8 form an air-spaced right angle prism. The center of the returning THz beam on mirror M6 is 30.5 cm above the center of the outgoing THz beam on M6. The returning THz beam is reflected horizontally by M6 to the upper mirror M9 shown in the insert, which reflects the beam back to mirror M4 with a $-1.25°$ (21.8 mrad) vertical tilt down to optimize coupling to the THz receiver. The returning beam maintains the 1.25° vertical tilt after the reflection by M4 to the center of the focusing mirror M3. The focusing reflection of the returning beam by M3 also maintains

the downward tilt and thereby directs the focus to M10 after the reflection by M2. The reflection from M10 removes the vertical tilt φ and directs the beam horizontally into the receiver for the excellent coupling, which is determined by the overlap integral [21] between the frequency-dependent Gaussian beam-waist of the receiver and the diffraction limited focus of the incoming beam, by the 32-cm (12.5-in)-diameter mirror 318 cm (125 in) away.

This THz optical train involving two horizontal planes separated from each other by 30.5 cm is relatively straightforward to set up and to align; it provides excellent optical coupling from the transmitter through the 167-m-long optical path and back into the receiver. The coupling mirrors M1 and M10 are on a three-ball bearing-supported magnetic mounting assembly, which can be easily removed and reinstalled with no mirror alignments required.

The THz optical train of Fig. 3 has several features to increase the strength of the transmitted signal at the receiver. First, M3 is a large 32-cm (12.5-in)-diameter telescope mirror; and the focal point of M3 is located at the Gaussian beam waist of the THz transceiver. Consequently, M3 collimates the THz beam, which gently expands by diffraction as it traces the optical path. The measured outgoing Gaussian amplitude 1/e diameters at M3 are 15 cm (6 in) at 1 THz, 20 cm (8 in) at both 0.5 and 0.25 THz. Using the measured diameters at M3, the outgoing diffracted Gaussian beam diameters are calculated at M6 to be 18.3 cm (7.2 in) at 1 THz, 25.4 cm (10 in) at 0.5 THz, and 29.5 cm (11.6 in) at 0.25 THz; at M7, they have diffracted to 25.6 cm (10.2 in) at 1 THz, 37.4 cm (14.7 in) at 0.5 THz, and 66 cm (26 in) at 0.25 THz, and for the incoming beam at M3, they have diffracted to 44.3 cm (17.5 in) at 1 THz, 65.4 cm (25.8 in) at 0.5 THz, and 126.4 cm (49.8 in) at 0.25 THz.

We use large, optical-quality mirrors with Enhanced Aluminum coatings to guide the THz beam; the Enhanced Aluminum coatings from Edmund Optics consist of a multilayer dielectric film on top of the aluminum, which enhances the visible reflectivity for our initial alignment with a 15-mW HeNe laser. The large mirror sizes are M4 is 40.6 cm $\times$ 40.6 cm (16 in $\times$ 16 in); M5 is 30.5 cm $\times$ 30.5 cm (12 in $\times$ 12 in); M6–M8 are 40.6 cm wide $\times$ 61 cm tall (16 in $\times$ 24 in), and M9 is 61 cm wide $\times$ 40.6 cm tall (24 in $\times$ 16 in).

Another experimental consideration is that for the humid air case, what is the effect of a thin 100-nm layer of adsorbed water on the reflectivity of mirrors M1–M10, all with enhanced aluminum coatings [10]. For the essentially normal incidence on mirrors M3, M4, and M6, the total E field is zero at the surface independent of polarization; consequently, the water layer has negligible absorption [10]. The same situation would hold for the vertical 45° mirrors M1, M2, M7, M8, and M10, with horizontal polarization, which is our case. However, there could be loss from the horizontal 45° mirrors M5 and M9. The considered double-pass amplitude absorption through the 100-nm water layer on mirrors M5 and M9 would be less than $\exp -[400\text{ nm} \times 200\text{ cm}]/2 = 0.4\%$, for which the power THz absorption coefficient of liquid water was assumed to be 200/cm. Fortunately, this upper limit gives a relatively small effect.

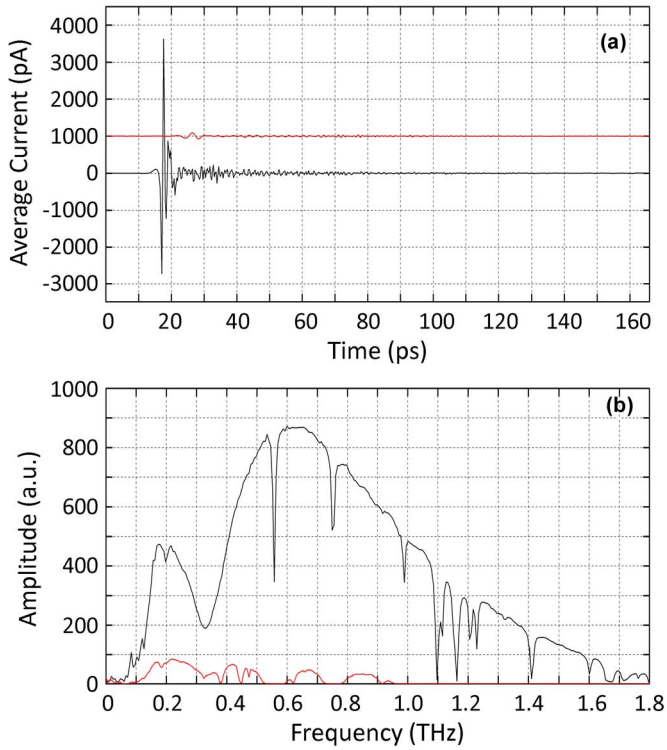

Fig. 4. (a) Measured THz input pulse (lower trace) and measured THz output pulse (upper trace) from the 167-m long path with RH 51% at 21 °C, also shown with an expanded vertical scale in Fig. 2. For clarity the output pulse has been shifted upwards by 1000 pA. (b) Corresponding amplitude spectrum for THz input pulse (upper curve) and the amplitude spectrum of the output pulse (lower curve), also shown with an expanded scale in Fig. 5.

The measurement sequence is as follows. First, system operation and stability are checked by measuring the performance of the THz-TDS system with the coupling mirrors removed. This measurement gives the input pulse to mirror M1 at the start of the long path. Second, the coupling mirrors are reinstalled (with no mirror realignment required), and the THz output pulses, transmitted through the entire system are measured. Then, system operation and stability are again checked by measuring the input pulse with the coupling mirrors removed. This sequence is repeated several times during the complete transmission measurement.

As shown in Fig. 4, the input and output pulses are measured over a scan duration of 165 ps, corresponding to the frequency resolution of 6.1 GHz. A scan consists of 625 channels (data points) with 40-μm steps between channels, corresponding to the double-pass (80 μm) time step of 0.2664 ps between channels. A single scan takes 180 s. Typically, four input pulses and four output pulses were measured, and then zero-padded to a total scan length of 1650 ps. The input THz beam was mechanically chopped at 348 Hz, and lock-in detection with an integrating time constant 100 ms was used.

The amplitude spectra of these zero-padded pulses were obtained from their complex Fourier transforms and were then averaged together to obtain the final amplitude spectra. Fig. 4(a) compares the averaged input pulse to the averaged output pulse. The input pulse appears quite clean with little oscillation due to the much smaller 50-cm path in the atmosphere. When the input pulse is coupled to the long 167-m path in laboratory air with

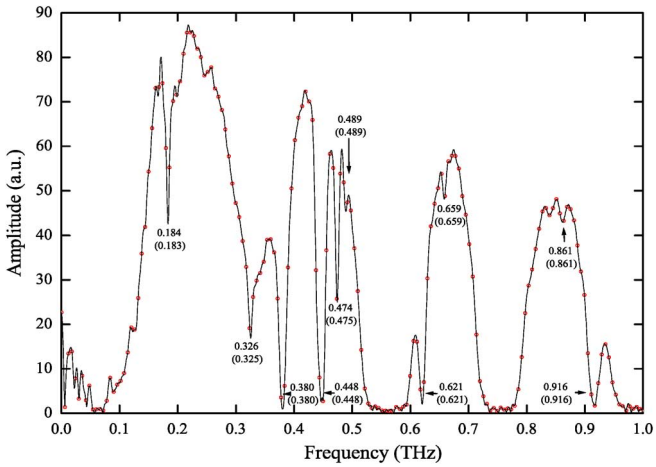

Fig. 5. Amplitude spectrum of THz pulse transmitted through a 167-m path in laboratory air with RH 51% at 21 °C. The "real data points" are indicated by the open circles, separated from each other by 6.1 GHz; the interpolated points obtained from the zero-padding are separated from each other by 0.61 GHz and define the solid line. The handbook frequencies are in parentheses.

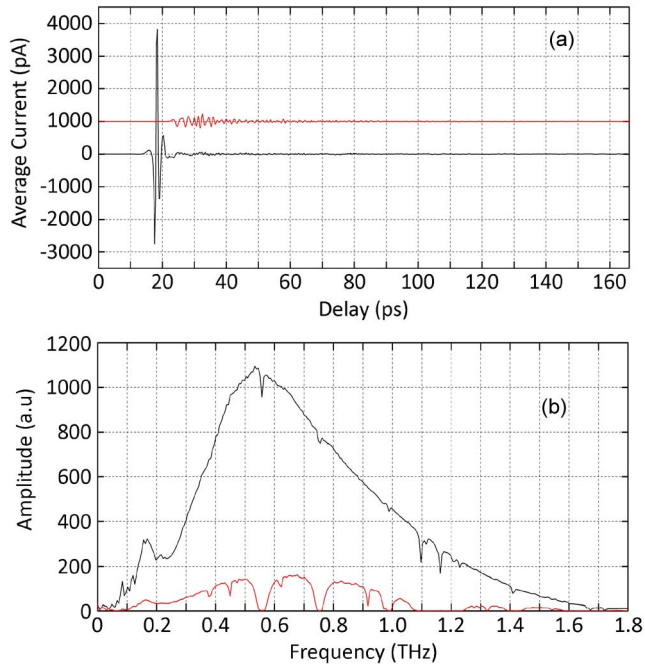

Fig. 6. (a) Measured THz input pulse (lower trace) and measured THz output pulse (upper trace) from the 167 m long-path with RH 4% at 21 °C, also shown with an expanded scale in Fig. 7(a). For clarity the output pulse has been shifted upwards by 1000 pA. (b) Corresponding amplitude spectrum for THz input pulse (upper curve) and the amplitude spectrum of the output pulse (lower curve), also shown with an expanded scale in Fig. 7(b).

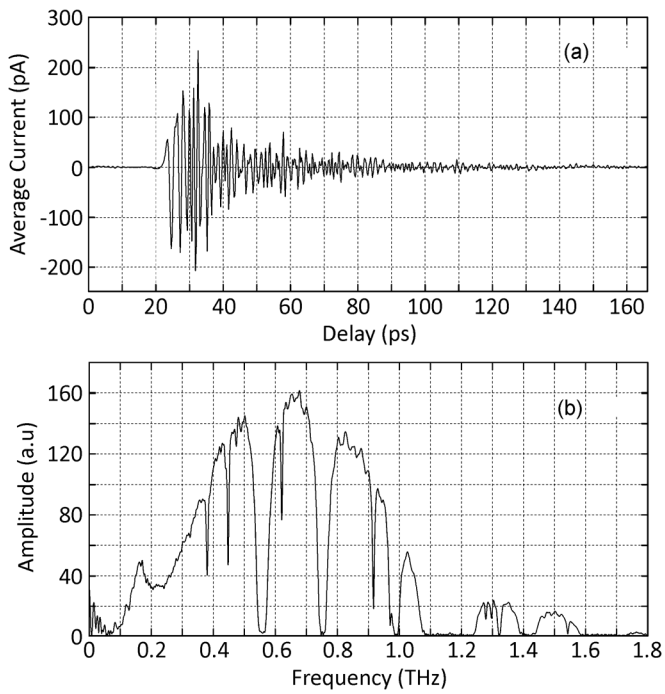

Fig. 7. (a) Measured THz pulse transmitted through the 167-m path with RH of 4% at 21 °C. (b) Corresponding amplitude spectrum of the THz transmitted pulse. Note the reduced absorption line strengths compared to Fig. 5.

RH 51% at 21 °C, the output pulse shows very strong and extended ringing from the rotational lines of water vapor in Fig. 2, which has an expanded vertical scale compared to Fig. 4(a). The comparison of the averaged input and averaged output amplitude spectra is shown in Fig. 4(b). The input spectrum completely shows the strong water lines, indicating the much shorter 50-cm path in the THz-TDS system. In contrast, in Fig. 4(b) and Fig. 5, the output spectrum shows complete absorption bands for the strong water lines and the significant appearance of the very weak water lines at their handbook frequencies and with resolution limited linewidths.

Fig. 5 shows [with an expanded vertical scale compared to Fig. 4(b)] the amplitude spectrum of the long-path pulse with the weak water lines clearly displayed and identified to a precision of 1 GHz, illustrating the power of THz sensing of vapors. The line frequencies in parentheses are the handbook values. The measured linewidths are equal to the spectral resolution of 6.1 GHz, which is determined by the time domain scan length of 165 ps. The complete absorption bands are produced by the strong water lines. The transmission of the spectral windows illustrates the THz potential for ranging, imaging, communications, and sensing in the range of a few hundred meters [3], [4].

III. Determination of the Amplitude Coupling Ratio

In order to understand the measurements in more detail and to separate the effects due to water vapor from the amplitude coupling ratio of the THz optical train, we have made a measurement at the lowest relative humidity obtainable due to seasonal changes and the consequent changing laboratory humidity. The measurements shown in Figs. 6 and 7 were taken with RH 4% at 21 °C and give a first approximation to the dry-air amplitude coupling ratio.

Comparing the measured transmitted RH 4% pulse in Fig. 7(a). to the RH 51% pulse in Fig. 2, the maximum to minimum feature of 450 pA is clearly larger than the corresponding 170-pA feature for the RH 51% pulse. The features on the RH 4% pulse oscillate at much higher frequencies than for the RH 51% pulse, due to the spectrum of the RH 4% pulse extending all the way out to 1.6 THz with reasonable strength, compared to that for the RH 51% pulse, which is cut off at 0.95 THz by the extra water vapor absorption. Note that for Fig. 7(a), the

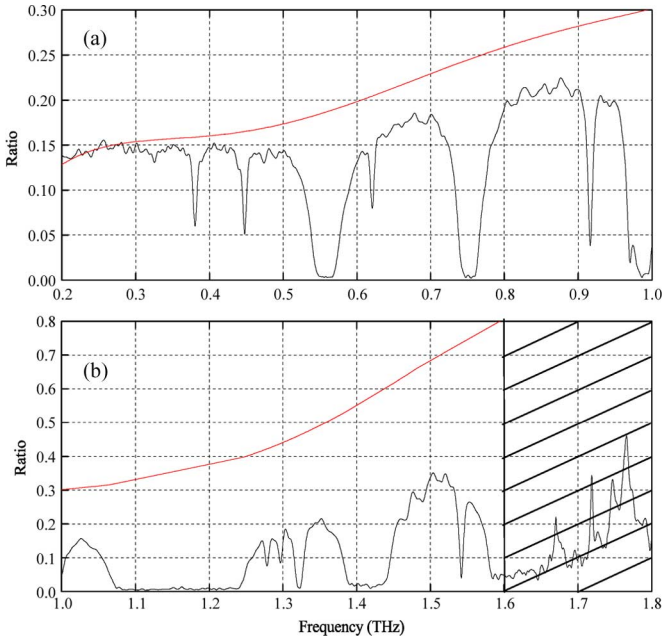

Fig. 8. ACR of the long-path THz optical train consisting of the round-trip defined by mirrors M1–M10 as shown in Fig. 3. The ACR shown is the ratio of the amplitude spectrum of the output pulse to that of the input pulse for the RH 4% measurement shown in Fig. 6(b). The monotonically increasing upper lines are the dry-air ACR, obtained after removing the effect of water vapor absorption. The ACR is equal to the square root of the power coupling efficiency [21].

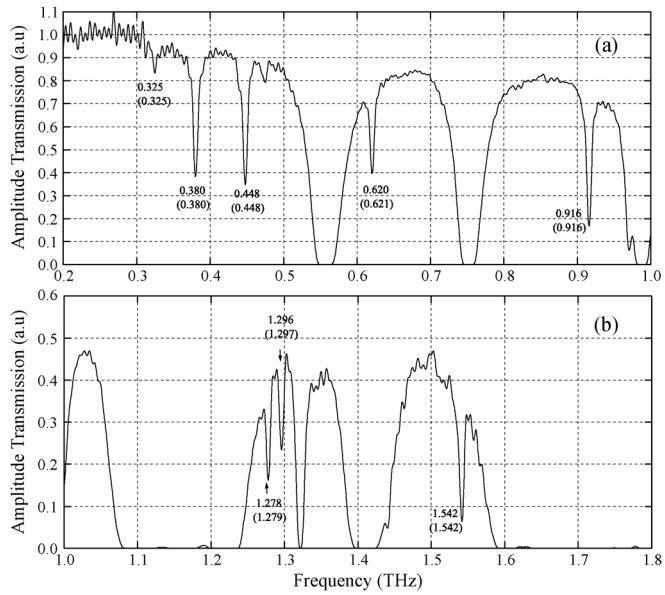

Fig. 9. The predicted amplitude transmission for the 167 m path in the atmosphere with a RH 7.0%. This prediction is based on data from the recent precision measurement of water vapor absorption [18], scaled to match our measured absorbance of the 0.380 THz line in Figs. 7(b) and 8(a).

characteristic long-path pulseshape of an initial pulse followed by an extensively broadened and frequency swept trailing edge, was not established, due to the much smaller GVD for RH 4%.

Fig. 8 shows the resulting amplitude coupling ratio (ACR), which is the ratio of the output amplitude spectrum to the input amplitude spectrum in Fig. 6(b). Although the water absorption has been much reduced compared to Fig. 5, it clearly dominates the measured ACR for frequencies above 1 THz. Between 0.1 and 1 THz, the measured ACR is between 0.15 and 0.2, increasing with frequency up to 0.35 at 1.5 THz. ACR is equal to the square root of the power coupling efficiency [21]. The smooth upper ACR curves show the dry-air ACR, obtained after the removal of the water vapor absorption. The dry-air ACR results are quite good and show the excellent coupling between the transceiver and the 167-m long path, 10-mirror optical train.

IV. Obtaining the Dry-Air ACR

We now discuss our procedure for eliminating the effect of water vapor absorption to obtain the resulting dry-air ACR (upper curves) shown in Fig. 8. Even though our ACR measurement was made at the low RH 4% at 21 °C, there is clearly much attenuation due to water vapor. We have recently characterized atmospheric water vapor absorption from 0.2 to 2 THz with a 6.2-m path length at RH 51% and 21 °C [18], and these results can be used to determine the effect of water vapor absorption on our ACR measurement.

Using a scaling procedure on the measured data of [18], we generate the predicted scaled amplitude transmission of the atmosphere for our long-path system in Fig. 9(a) and (b), which matches the measured absorbance for the well-resolved water line at 0.380 THz in Figs. 7(b) and 8(a). The transmission prediction was made by first calculating the amplitude absorbance $= -\ln(\mathrm{A_2}/\mathrm{A_R})$ of the line at 0.380 THz in Fig. 8(a) to be 0.89, where $\mathrm{A_2}$ is the measured minimum amplitude at line center and $\mathrm{A_R}$ is the estimated baseline drawn over the line feature. Then, 0.89 will be compared to the absorbance for the same water line measured in the amplitude transmission of a 6.2-m path of atmospheric water vapor at RH 51% [18], which has the value of 0.24.

To increase the amplitude absorbance from 0.24 to 0.89, the measured transmission of [18] is taken to the $0.89/0.24 = 3.71$ power, i.e., $(\text{amplitude transmission})^{3.71}$. Here, we use the linear relationship between absorbance, length and RH (for constant temperature); the absorbance (for the weak water lines) is proportional to length $\times$ RH. Thus, to match the absorbance of 0.89 we have $(6.2)(3.71) = 23.0$ m path at RH 51%, or equivalently a 230-m path at RH 5.1%. These results require our low-humidity path of 167 m to have the higher RH 7.0%, compared to our measured value of 4%. Such low levels of humidity are measured imprecisely with standard instruments with specifications of $\pm 1.5\%$, regardless of humidity value. Consequently, RH 7.0% is considered to be the more accurate value.

The above procedure to obtain Fig. 9 is precise for the absorption line strengths. It does, however, overestimate the continuum absorption (Curve B in Fig. 1), which increases as the square of the humidity. However, the attenuation shown in Fig. 9(a) between 0.2 to 0.3 THz is already insignificant, and the correction between 0.3 and 0.5 THz would only be a few percent.

For frequencies above 0.5 THz, the continuum absorption is a relatively small component of the total absorption in the windows of transparency between the strong water lines. Consequently, Fig. 9 is considered to be of adequate accuracy for our water vapor absorption correction to the ACR described below.

In principle, to take out the effect of water vapor absorption from the ACR shown in Fig. 8(a) and 8(b); all that needs to be done is to divide Fig. 8(a) and (b) by Fig. 9(a) and (b), respectively. However, this gives results with unacceptable scatter. Consequently, we smoothed Fig. 9(a) and (b) and eliminated the numerical singularities by replacing the regions of very low transmission in Fig. 9(a) and (b) by regions of constant 0.1 transmission. Dividing 8(a) and (b) by this smoothed version of 9(a) and (b), we obtained corrected ACR results, which were well fit by the simple monotonically increasing dry-air ACR curves shown in Fig. 8(a) and (b). These smoothly increasing dry-air ACR curves show the quite good coupling of the THz beam train to the THz transceiver.

V. Estimation of Diffraction Effect on ACR

The dry-air ACR curves in Fig. 8 include the diffraction loss, which is part of the characteristics of our system. A relatively simple argument can be made to estimate the effect of diffraction on these results. As noted earlier, the measured outgoing Gaussian amplitude 1/e diameters at M3 are 15 cm at 1 THz and 20 cm at 0.5 THz and 0.25 THz. Considering only the simple diffraction of the collimated outgoing beam from M3 for the round-trip distance of 160.9 m back to M3, the calculated diffracted amplitude Gaussian beam diameters have become 44.5 cm at 1 THz, 65.4 cm at 0.5 THz, and 126.4 cm at 0.25 THz. Assuming that all the reflections involved in the round-trip back to M3 occur without loss, that the mirrors M4–M9 are large enough to reflect the entire diffracting beam, and that all of the returning power incident on M3 is coupled without loss into the THz receiver, we can make the following reasonable estimate.

First, the calculated power capture fraction $\mathrm{F_p}(\omega)$ of the frequency-dependent returning round-trip power incident on the 32-cm-diameter focusing mirror is given simply by the Gaussian optics result $\mathrm{F_p}(\omega) = 1 - \exp(-2\ \mathrm{a}^2/\mathrm{w}^2)$, where 2a is the diameter of the aperture (focusing mirror) and 2w is the returning diffracted Gaussian beam diameter. Evaluating this expression for our values, we obtain for the power capture fraction $\mathrm{F_p} = 0.660$ for 1 THz; $\mathrm{F_p} = 0.388$ for 0.5 THz, and $\mathrm{F_p} = 0.124$ for 0.25 THz. For the corresponding amplitude coupling effect of diffraction $\mathrm{F_a} = (\mathrm{F_p})^{1/2}$, and we thereby obtain $\mathrm{F_a} = 0.812$ at 1 THz; $\mathrm{F_a} = 0.623$ at 0.5 THz, and $\mathrm{F_a} = 0.352$ at 0.25 THz. Consequently, if we could remove this diffraction loss $\mathrm{F_a}(\omega)$ from the system, the dry-air ACR curves shown in Fig. 8 would increase by $1/\mathrm{F_a}(\omega)$. For example, at 0.25 THz, the dry-air ACR curve would increase by the factor of 2.84.

VI. Observation of the THz Bit Pulse

A careful study of the transmitted THz pulses through 167 m of humid air has revealed the THz bit pulse for digital (binary) communications. As shown in Fig. 10(a), the almost completely separated initial low-frequency pulses of the frequency swept and broadened RH 40% and RH 50% transmitted pulses, appear to be propagating with little loss and distortion. The time separation and the relatively more severe attenuation of the higher frequency components are clearly shown by comparison to the

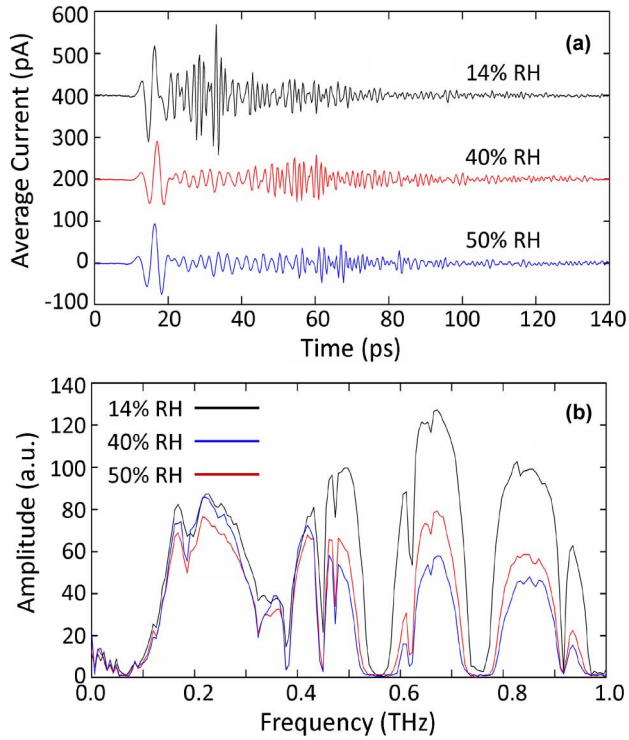

Fig. 10. (a) Measured THz pulses transmitted through the 167-m path with RH 14%, RH 40% and RH 50%. (b) Corresponding amplitude spectra of the transmitted pulses. RH 40% refers to the lowest curve at 0.2 THz; RH 14% refers to the highest curve at 0.7 THz; and RH 50% refers to the lowest curve at 0.85 THz.

RH 14% pulse. The stable pulsewidth is composed of the frequency components within the 0.07–0.37-THz range of the presented amplitude spectra.

One can understand the formation and revealing of the THz bit pulse in the following way. The initial optical excitation pulse of the transmitter generates the initial short input THz pulse, for which the frequency components of the input amplitude spectrum are initially all in phase. During propagation through the long path of the atmosphere, the higher frequency components are much more attenuated and have significantly slower group velocities. Consequently, the frequencies separate in time with the higher frequencies extending the pulse train. The initial 0.5-ps input pulse changes to a ringing, frequency swept, output pulse extending to as much as 160 ps with the highest frequency at the end of the pulse. In addition, the higher frequencies are much more attenuated by the water vapor, so that the lowest frequency components of the output pulse appear together at the front of the pulse with very little attenuation and very little broadening by group velocity dispersion. Finally, for very long paths with high humidity, only the ideal pulse shape remains. The symmetric shape of the THz bit pulse shows that all of the frequency components are in phase.

To provide conclusive evidence that the lower frequency THz components keep their initial phase coherence, while propagating through the 167-m long path, we have numerically calculated the RH 50% output pulse (IFFT) from the experimental RH 50% amplitude spectrum between 0.07 and 0.37 THz of Fig. 10(b), assuming that all of the frequency components are in phase. The calculated phase coherent output pulse is shown in

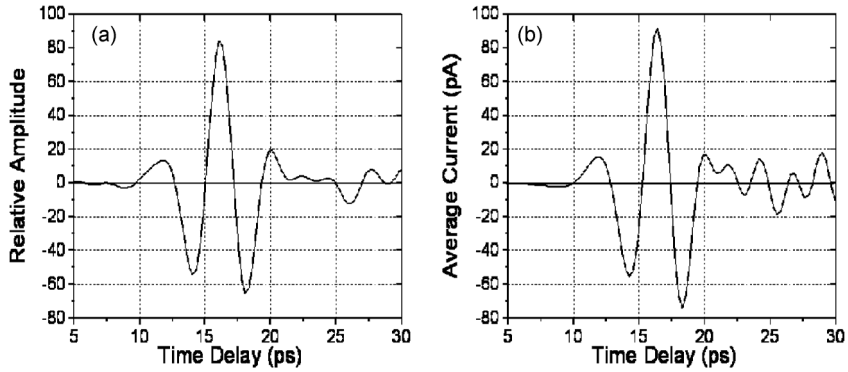

Fig. 11. (a) Calculated coherent THz output pulse, assuming an in-phase frequency spectrum given by the measured RH 50% amplitude spectrum from 0.07 to 0.37 THz shown in Fig. 10(b). (b) Measured THz bit pulse on the leading edge of the RH 50% output pulse shown in Fig. 10(a).

Fig. 11(a) and can be compared to the experimentally observed THz bit pulse on the leading edge of the RH 50% output pulse, shown in Fig. 11(b) on the same time scale for comparison. The similarity of these two pulses confirms the coherence and low GVD for the propagating THz bit pulse. The THz bit pulse consists of two damped cycles of 250-GHz oscillation, centered on the cosine peak. This pulseshape is ideal for homodyne detection with a 250-GHz local oscillator, which with mixing will rectify the pulseshape, giving a product of the THz bit pulse amplitude and the amplitude of the local oscillator.

Our resulting prediction is that the THz bit pulse would become more defined and relatively much larger than the much more attenuated higher frequency features, if the long path of 167 m would be significantly extended, perhaps doubled. The water vapor absorption is quite low in the 0.07–0.37-THz frequency range, so low that it could not be measured in the in the long-tube experiment [18]. Consequently, there is the possibility of a useful 1-km path length for this single THz bit pulse. It should be clear that the low-power THz transceiver used to perform these measurements is well suited to test the atmospheric THz digital communications channel.

Based on the realized 167-m transmission shown in Fig. 10, the bit rate–distance product is competitive with the early second-generation optical fiber channel, as will now be discussed. If we assume a bit stream of these pulses well separated from each other by 20 ps, we obtain a bit rate of 50 Gb/s. This result, together with the measured distance of 0.167 km, gives the impressive bit rate–distance product of this THz communication channel of 8.3 (Gb/s)-km. This result is competitive with that of the second-generation optical fiber channel with a bit rate–distance product of 10 (Gb/s)-km as shown in the early optical measurement [22] presented in Fig. 12. It is interesting to note that the THz bit pulse is a symmetric field pulse, while the optical bit pulse is an unsymmetrical power envelope pulse of the much higher frequency optical carrier. Finally, it should be emphasized that our demonstrated product is only a lower limit, the attainable value could be much higher. We plan to test this by new measurements with much longer paths.

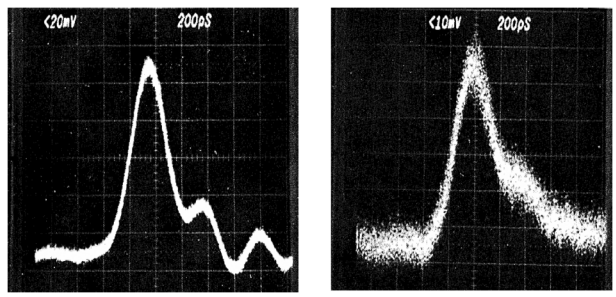

Fig. 12. Early (1978) demonstration of a digital optical fiber communications channel with a 10 (Gb/s)-km bit rate–distance product [22]. Left panel: Measured input optical pulse to a 10.4-km single-mode optical fiber. Right panel: Measured output optical pulse. Measurements were made with a sampling oscilloscope with a horizontal scale of 200 ps/div. The optical source was an InGaAsP/InP laser with wavelength of 1.293 μm. The measured input pulsewidth was 315 ps, and the measured output pulsewidth was 355 ps. This figure is a modified version of Fig. 1 of [22].

VII. Discussion and Summary

We have demonstrated the transmission of an input 30-nW low-power beam of repetitive broadband THz pulses through the record, round-trip path of 167 m through the atmosphere at RH 51% at 21 °C and have observed the broadened output THz pulses with an S/N greater than 200. The repetitive optoelectronic transceiver is phase coherent and, thereby, could measure the 120-pw reduced-power output beam with such high S/N. The amplitude coupling ratio (ACR) of the 10-mirror, 14-reflection system was quite acceptable and was mainly limited by diffraction loss. The measured ACR monotonically increased with frequency, from ACR = 0.14 at 0.2 THz to 0.2 at 0.6 THz to 0.3 at 1 THz, to 0.5 at 1.35 THz and to 0.8 at 1.6 THz.

The corresponding amplitude spectrum extending from 0.1 to 1 THz of the long-path THz pulse clearly shows the weak and the very weak water lines. These lines were measured with a precision of 1 GHz, clearly demonstrating the ability to sense harmful vapors with frequency precision and exceptional sensitivity [23]. It is of interest to note that all of the resonance lines shown in Figs. 4(b), 5, 6(b), 7(b), and 9 are water vapor lines. There was no THz sensing evidence of any other molecular vapors in our laboratory.

If we had long-term experimental stability over many days, it would be possible with our long path system to obtain exceptionally accurate measurements of the water vapor absorption in the transparency windows between the water absorption lines. The measurement would be similar to that described in [18], except we would use the ratio of transmitted spectra with different humidity instead of the ratio between the transmitted spectrum to that with a controlled extremely low level of humidity of less than RH 0.5%. For example, with long-term stability, the ratios

of the RH 51% spectrum shown in Figs. 4 and 5 to that of the RH 4% transmitted spectrum shown in Fig. 7, both at 21 °C would provide the water vapor absorption corresponding to RH 47% at 21 °C. However, the long-term changes in our pumping laser and in the amplitude coupling ratio of the long-path system were always too much to allow the ratio of such measurements to obtain the desired accuracy.

The measured transmitted pulses reshaped from a 0.5-ps input pulse into an output pulse structure with a 5-ps symmetric pulse at the leading edge followed by a frequency swept rapidly oscillating trailing edge extending with increasing frequency to beyond 150 ps. The leading pulse in the output pulse structure was composed of phase-locked frequency components extending from 0.07 to 0.37 THz, which experienced negligible attenuation and GVD due to transmission through water vapor. Such a stable pulseshape could be the THz bit in a digital THz communications channel. These results demonstrate a bit rate–distance product of greater than 8 (Gb/s)-km, which is comparable to an optical fiber digital communications channel.

Our demonstration of the atmospheric THz digital communications channel should not be confused with a demonstration of a THz digital communications system, which requires the development of a new type of THz transmitter and THz bit receiver. In order to use the full capability of the demonstrated THz channel, the THz transmitter would need to be able to digitally switch out one or zero 5-ps THz pulses at the bit rate of 50 GHz, where a one bit is a pulse and a zero bit is no pulse. The receiver would have to operate at 50 GHz with the capability of measuring pulse or no pulse with a bit error rate of 10^{-6}. Such a system would have the capability of delivering an immense amount of information in a short time.

We predict that the observed THz bit pulse would become more defined and relatively much larger than the much more attenuated higher frequency features, if the long-path of 167 m would be significantly extended, perhaps doubled. Water vapor absorption is quite low in the 0.1–0.3-THz frequency range; thereby, there is the possibility of a useful 1-km path length for this single bit pulse. We plan to test this prediction by doubling the path-length. In addition, by changing optoelectronic transmitter and receiver antennas to enhance and compress the frequency band to 0.1–0.35 THz, we plan to generate much stronger THz bit pulses and to detect them with more sensitivity. In our opinion, these results demonstrating the THz digital communications channel show significant promise for THz free-space communications and vapor sensing applications.

ACKNOWLEDGMENT

The authors acknowledge careful readings of this manuscript by J. S. Melinger, J. O'Hara, and Yuping Yang.

REFERENCES

[1] *Atmospheric Water Vapor*, A. Deepak, T. D. Wilkerson, and L. H. Ruhnke, Eds.. New York: Academic, 1980, Proceedings of the 1979 Int. Workshop on Atmospheric Water Vapor.

[2] "The DARCOM/DARPA Near-Millimeter Wave Technology Base Study," The Defense Technical Information Center, 1978, vol. I–III [Online]. Available: http://www.dtic.mil/cgi-bin/GetTRDoc? Location=U2&doc=GetTRDoc.pdf&AD=ADA079620

[3] P. H. Siegel, "Terahertz technology," *IEEE Trans. Microw. Theory Tech.*, vol. 50, pp. 910–928, Mar. 2002.

[4] R. Appleby and H. B. Wallace, "Standoff detection of weapons and contraband in the 100 GHz to 1 THz region," *IEEE Trans. Antennas Propag.*, vol. 55, pp. 2944–2956, Nov. 2007.

[5] D. E. Burch and D. A. Gryvnak, "Continuum absorption by water vapor in the infrared and millimeter regions," in *Atmospheric Water Vapor*. New York: Academic, pp. 47–76, Proceedings of the Int. Workshop on Atmospheric Water Vapor.

[6] Y. A. Dryagin, A. G. Kislyakov, L. M. Kukin, A. I. Naumov, and L. I. Fedosyev, "Measurement of the atmospheric absorption of radio waves in the range 1.36–3.0 mm," *Isv. Vyssh. Uchebn. Zaved. Radiofiz.*, vol. 9, pp. 627–644, 1966.

[7] R. L. Frenkel and D. Woods, "The microwave absorption by H_2O and its mixtures with other gases between 100 and 300 Gc/s," *Proc. IEEE*, vol. 54, pp. 498–505, 1966.

[8] A. W. Straiton and C. W. Tolbert, "Anomalies in the absorption of radio waves by atmospheric gases," *Proc. IRE*, vol. 48, pp. 898–903, 1960.

[9] V. Y. Ryadov and N. I. Furashov, "Investigation of the spectrum of radiowave absorption by atmospheric water vapor in the 1.15 to 1.5 mm range," *Radio Phys. Quantum Electron.*, vol. 15, pp. 1124–1128, 1974.

[10] D. E. Burch, D. A. Gryvnak, and R. R. Patty, "Absorption of infrared radiation by CO_2 and H_2O. experimental techniques," *J. Opt. Soc. Amer.*, vol. 57, pp. 885–895, 1967.

[11] D. E. Burch, "Absorption of infrared radiant energy by CO_2 and H_2O. III. Absorption by H_2O between 0.5 and 36 cm^{-1}," *J. Opt. Soc. Amer.*, vol. 58, pp. 1383–1394, 1968.

[12] M. van Exter, C. Fattinger, and D. Grischkowsky, "Terahertz time-domain spectroscopy of water vapor," *Opt. Lett.*, vol. 14, pp. 1128–1130, 1989.

[13] M. van Exter and D. Grischkowsky, "Characterization of an optoelectronic TeraHz beam system," *IEEE Trans. Microw. Theory Tech.*, vol. 38, pp. 1684–1691, Nov. 1990.

[14] D. Grischkowsky, S. Keiding, M. van Exter, and C. Fattinger, "Far-infrared time-domain spectroscopy with terahertz beams of dielectrics and semiconductors," *J. Opt. Soc. Amer. B*, vol. 7, pp. 2006–2015, 1990.

[15] T. Yuan, H. B. Liu, J. Z. Xu, F. Al-Douseri, Y. Hu, and X.-C. Zhang, "Terahertz time-domain spectroscopy of the atmosphere with different humidity," in *Proc. SPIE*, 2003, vol. 5070, no. 1, pp. 28–37.

[16] S. Wohnsiedler, M. Theuer, M. Herrmann, S. Islam, J. Jonuscheit, R. Beigang, and F. Hase, "Simulation and experiment of Terahertz stand-off detection," in *Proc. SPIE*, 2009, vol. 7215, p. 72150H.

[17] H. B. Liu, H. Zhong, N. Karpowicz, Y. Chen, and X.-C. Zhang, "Terahertz spectroscopy and imaging for defense and security applications," *Proc. IEEE*, vol. 95, no. 8, pp. 1514–1527, Aug. 2007.

[18] Y. Yang, A. Shutler, and D. Grischkowsky, "Measurement of the transmission of the atmosphere from 0.2 to 2 THz," *Opt. Exp.*, vol. 19, pp. 8830–8838, 2011.

[19] S. E. Ralph and D. Grischkowsky, "THz spectroscopy and source characterization by optical interferometry," *Appl. Phys. Lett.*, vol. 60, pp. 1070–1072, 1992.

[20] F. E. Doany, D. Grischkowsky, and C.-C. Chi, "Carrier lifetime vs ion-implantation dose in silicon on sapphire," *Appl. Phys. Lett.*, vol. 50, pp. 460–462, 1987.

[21] J. E. G. Lesurf, *Millimetre-Wave Optics, Devices & Systems*. Bristol, U.K.: Adam Hilger, 1990.

[22] A. Kawana, M. Kawachi, T. Miyashita, M. Saruwatari, K. Asatani, J. Yamada, and K. Oe, "Pulse broadening in long-span single-mode fibers around a material-dispersion-free wavelength," *Opt. Lett.*, vol. 2, pp. 106–108, 1978.

[23] J. S. Melinger, A. Shutler, Y. Yang, and D. Grischkowsky, "Long path detection of small molecule vapors in the atmospheric transparency windows," presented at the CLEO 2011, Opt. Soc. Amer., Washington, DC, 2011, CThEE7.

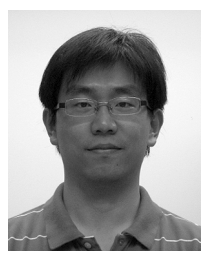

Yihong Yang (S'11) was born in Hebei, China, in 1983. He received the B.S. and M.S. degrees from Nankai University, Tianjin, China, in 2006 and 2009, respectively. Currently, he is working towards the Ph.D. degree in the School of Electrical and Computer Engineering, Oklahoma State University, Stillwater.

His current research interests include terahertz time-domain detection, broadband terahertz atmosphere propagation, and terahertz communication.

Mahboubeh Mandehgar received the B.S. degree from Azzahra University, Tehran, Iran, in 2003 and the M.S. degree from the University of Central Missouri in 2010. She is currently working towards the Ph.D. degree at the Oklahoma State University, Stillwater, working on THz spectroscopy and THz communication system.

Daniel R. Grischkowsky (SM'90–F'92) received the B.S. degree from Oregon State University, Corvallis, in 1962 and the Ph.D. degree from Columbia University, New York, in 1968.

In 1969, he joined the IBM Watson Research Center, Yorktown Heights, NY. In 1993, he joined Oklahoma State University, Stillwater, where his work has concentrated on unique applications of THz–TDS, including waveguides, the Sommerfeld wave, surface waves, hole arrays, and photonic crystals.

Dr. Grischkowsky is a Fellow of the Optical Society of America (OSA) and the American Physical Society. He was awarded the 1985 Boris Pregel Award by the NY Academy of Sciences, the OSA 1989 R. W. Wood Prize, the OSA 2003 William F. Meggers Award, and the 2011 Kenneth J. Button Prize from the International Society of IR, MM and THz Waves.